



Contents lists available at SciVerse ScienceDirect

## Remote Sensing of Environment

journal homepage: [www.elsevier.com/locate/rse](http://www.elsevier.com/locate/rse)

# Spatio-temporal patterns of chlorophyll fluorescence and physiological and structural indices acquired from hyperspectral imagery as compared with carbon fluxes measured with eddy covariance

P.J. Zarco-Tejada<sup>a,\*</sup>, A. Morales<sup>a,b</sup>, L. Testi<sup>a</sup>, F.J. Villalobos<sup>a,c</sup><sup>a</sup> Instituto de Agricultura Sostenible (IAS), Consejo Superior de Investigaciones Científicas (CSIC), Córdoba, Spain<sup>b</sup> Plant Production Systems Group, Wageningen University, P.O. Box 430, 6700 AK Wageningen, The Netherlands<sup>c</sup> Departamento de Agronomía, Universidad de Córdoba, Campus Universitario de Rabanales, 14014 Córdoba, Spain

## ARTICLE INFO

## Article history:

Received 4 November 2012

Received in revised form 4 February 2013

Accepted 7 February 2013

Available online xxxx

## Keywords:

Hyperspectral

Physiological indices

Eddy covariance

Chlorophyll

Narrow-band indices

Gross primary production

GPP

Unmanned aerial vehicle

UAV

## ABSTRACT

This study provides insight into the assessment of the spatio-temporal trends of chlorophyll fluorescence, narrow-band physiological indices, and structural indices acquired with a hyperspectral imager flown over a flux tower in a canopy characterized by small seasonal structural changes and a heterogeneous architecture. A total of seven flights between summer and autumn were conducted with a hyperspectral camera that captured 30 cm resolution imagery and 260 spectral bands in the 400–900 nm region. This enabled the identification of pure-vegetation tree crown pixels around an eddy covariance flux tower without shadow components or background effects. The hyperspectral imagery was used to study the temporal patterns of canopy fluorescence and reflectance indices related to physiology and canopy structure. The seasonal trends observed in the airborne indices and fluorescence and their relationship with gross primary production (GPP) demonstrated that vegetation indices mostly related to structure such as the normalized difference vegetation index (NDVI) and the enhanced vegetation index (EVI) yielded non-significant relationships ( $r^2=0.17$ ;  $p>0.05$ ) due to the small structural changes in the canopy through the season. By contrast, physiological indices related to chlorophyll content (TCARI/OSAVI), light use efficiency (PRI<sub>570</sub>), and canopy chlorophyll fluorescence calculated through the Fraunhofer Line Depth principle (FLD3) showed a similar seasonal trend to that of GPP measured at the same time of the flights ( $r^2$  in the range 0.75–0.84;  $p<0.01$ ). These results are consistent with the physiological trend observed during summer and autumn, which showed that chlorophyll content increased by 17.9% while the NDVI and the estimated tree crown projected LAI (LAI<sub>p</sub>) remained almost constant during the experiment (3% variation). The time-series hyperspectral dataset demonstrated that the seasonal trajectories of the NDVI and EVI were weakly related ( $p>0.05$ ) to the physiological indicators such as TCARI/OSAVI, PRI<sub>570</sub> and fluorescence. The spatial variability of the hyperspectral indices investigated through the coefficient of variation (CV) showed that fluorescence around the tower varied up to 17% at the time of the maximum stress (summer), while LAI<sub>p</sub> showed little variation during that time (CV = 1.8%). After the summer stress period, the CV for fluorescence and chlorophyll content decreased in autumn down to 9%. This study demonstrates that small physiological changes occurring in an evergreen canopy were still captured by remote sensing physiological indices and high-resolution airborne fluorescence. These indicators are required for GPP monitoring when the vegetation dynamics are not captured by remote sensing structural indices.

© 2013 Elsevier Inc. All rights reserved.

## 1. Introduction

Remote sensing research methods proposed for global monitoring of vegetation dynamics rely on vegetation indices related to canopy structure. Such indices include the normalized difference vegetation

index (NDVI) (Rouse et al., 1974) and other robust indices such as the enhanced vegetation index (EVI) (Huete et al., 2002), developed to avoid saturation at larger leaf area index (LAI) values and to be resistant to atmospheric effects. The NDVI, the EVI, and other vegetation indices mostly related to structure have been proposed in several studies as a proxy for LAI, canopy structure, green biomass, percent green cover, and fraction of absorbed photosynthetically active radiation (fAPAR) (Asrar et al., 1984; Baret & Guyot, 1991; Goward & Huemmrich, 1992; Huete et al., 2006; Jiang et al., 2008; Running & Nemani, 1988; Sellers, 1985). Certain models have identified these canopy parameters as being critical to scale up estimates of

\* Corresponding author at: Instituto de Agricultura Sostenible (IAS), Consejo Superior de Investigaciones Científicas (CSIC), Alameda del Obispo, s/n, 14004 – Córdoba, Spain. Tel.: +34 957 499 280, +34 676 954 937; fax: +34 957 499 252.

E-mail address: [pablo.zarco@csic.es](mailto:pablo.zarco@csic.es) (P.J. Zarco-Tejada).

URL: <http://quantalab.ias.csic.es> (P.J. Zarco-Tejada).

evapotranspiration, photosynthesis, primary production, and carbon balance (Running et al., 1999). Other earlier studies demonstrated that NDVI is related to carbon fixation and canopy resistance and have proposed this index as input for carbon models (Fung et al., 1987; Running et al., 1989).

Remote monitoring of net primary production (NPP) has been the target of several studies aimed at finding relationships with NDVI (and EVI) time series due to their sensitivity to seasonal phenological changes. As an example, early studies focused on the time integrals of NDVI over the growing season to show the correlations with net primary production (Justice et al., 1985; Prince, 1991; Running & Nemani, 1988; Tucker & Sellers, 1986). By contrast, Huete et al. (2006) tracked phenological changes in rainforests, showing relationships with gross primary production (GPP) and demonstrating the sensitivity of the EVI to changes in canopy photosynthetic capacity over the season.

The NDVI, the EVI, and other vegetation indices proposed to monitor vegetation dynamics are considered structural indices as they mostly track changes in canopy structure (see Haboudane et al., 2004 for a complete review) but have little or no sensitivity to short-term leaf physiological changes that are independent from the structure. Dobrowski et al. (2005) clearly demonstrated that the NDVI is not sensitive to diurnal physiological changes induced by heat and water stress and only tracks the effects in the long term. In evergreen crop canopies, such as olive and citrus orchards among others, NDVI-GPP or EVI-GPP relationships are restricted by the very small seasonal changes experienced by LAI and canopy structure. In particular, vegetation indices tracking canopy structure are not sensitive to physiological effects caused by heat and water stress or by absorbed light and canopy temperature. Therefore, using a remote sensing structural vegetation index as a proxy for GPP has certain limitations. The main drawback is that, in the EVI, for example, the index acts as a proxy for LAI, while GPP is a function of the actual single-leaf photosynthetic activity, which is affected by photosynthetic capacity and microclimatic factors that also fluctuate in the short term (Nagai et al., 2010). A critical limitation is that both leaf photosynthetic capacity and canopy LAI change seasonally (Muraoka & Koizumi, 2005) but these changes do not necessarily coincide in GPP and structural indices such as the EVI. Particularly in evergreen canopies, these physiological changes occur while canopy LAI remains unchanged. In the case of non-homogeneous canopies such as row-structured crops or in sparse vegetation, GPP predictions are less accurate when using EVI or MODIS GPP products due to large effects caused by shadows and background effects (Sims et al., 2008) which introduce substantial errors into the carbon exchange estimates.

There is a growing interest in improving the monitoring of the dynamics of vegetation physiology, including more accurate means of estimating GPP. In this context, new remote sensing methods are exploring indicators directly linked to diurnal changes in photosynthesis, such as chlorophyll fluorescence ( $F$ ), physiological indices related to light use efficiency (LUE), and chlorophyll content ( $C_{a+b}$ ) indices. In particular, chlorophyll fluorescence has been proposed as a direct indicator of photosynthesis, and several studies have demonstrated its relationship with vegetation functioning at the leaf, canopy, and airborne level (Krause & Weis, 1984; Lichtenthaler & Rinderle, 1988; Papageorgiou, 1975). This is based on the competition between steady-state fluorescence ( $F_s$ ) and photochemistry for excitation energy. Therefore,  $F_s$  may act as a potential means to track changes in the photosynthetic activity of vegetation via remote sensing (Flexas et al., 2000, 2002; Porcar-Castell, 2011; Soukupová et al., 2008).

As described earlier, leaf- and laboratory-level experiments have shown that fluorescence and narrow-band physiological reflectance indices are able to track diurnal changes caused by heat and water stress (Dobrowski et al., 2005). These studies have shown diurnal stress effects tracked by fluorescence extracted from canopy reflectance and detected by derivative indices (Zarco-Tejada et al., 2003).

In particular, fluorescence-sensitive reflectance indices measured at the canopy level were correlated with physiological measures such as steady-state fluorescence, tracking  $\text{CO}_2$  assimilation. The retrieval of the fluorescence signal is very complex, especially under natural light conditions, as the contribution to canopy radiance is estimated to be about 2–3%. Yet, several methods have been reported to extract the fluorescence signal at the leaf and canopy levels (Meroni et al., 2008a,b, 2009; Moya et al., 2004), which proves the feasibility of fluorescence retrieval using the  $\text{O}_2\text{-A}$  band feature.

The use of chlorophyll fluorescence as a direct proxy for photosynthesis has received attention for global monitoring purposes, and technical aspects and challenges have been discussed (Malenovsky et al., 2009). Such studies have mainly focused on scaling issues (Rascher et al., 2009) and on the modeling of GPP from fluorescence/assimilation rates in diurnal patterns (Damm et al., 2010). Part of these efforts were supported by the Fluorescence Explorer (FLEX) mission (European Space Agency, 2008), funded by the European Space Agency (ESA) Earth Explorer program. More recently, global maps of chlorophyll fluorescence have been published (Frankenberg et al., 2011; Joiner et al., 2011) using the thermal and near infrared sensor for carbon observation (TANSO) on board GOSAT (Kuze et al., 2009). An assessment found overall good agreement between fluorescence quantification by the satellite sensor and annual and seasonal vegetation patterns (Guanter et al., 2012).

These recent developments in the global mapping of fluorescence are critical steps forward. Yet, high-resolution validation experiments are needed to prove the validity of the fluorescence signal associated with photosynthesis in non-aggregated pure vegetation pixels (Zarco-Tejada et al., submitted for publication-a,b). Moreover, high-resolution hyperspectral imagery and ground validation fluorescence data are required to assess global-coverage low-resolution  $F_s$ /GPP relationships recently obtained from GOSAT and observed from future satellite platforms. This is critical, as vegetation structure, background, illumination, and atmospheric effects play a crucial role in fluorescence retrieval (Guanter et al., 2010; Zarco-Tejada et al., submitted for publication-a,b). Despite its importance, a limited number of validation studies have addressed the retrieval of fluorescence at high-resolution image level. Such slow progress is due to the lack of appropriate imagery acquired at very high spatial/spectral resolutions, the operational costs involved, and the complexity of acquiring proper field validation measurements. Recent studies (Zarco-Tejada et al., 2009) have applied the *in-filling* method to 1-nm airborne imagery, showing the feasibility of mapping fluorescence using an unmanned aerial vehicle (UAV) (Zarco-Tejada et al., 2012).

In addition to the efforts devoted to chlorophyll fluorescence retrieval, the physiological (or photochemical) reflectance index (PRI) (Gamon et al., 1992) has proven to be sensitive to the epoxidation state of xanthophyll cycle pigments. This is related to the light use efficiency of photosynthesis. Recent studies have proven the sensitivity of this index for vegetation stress detection and short-term physiology monitoring (Peguero-Pina et al., 2008; Suárez et al., 2008, 2009, 2010; Thenot et al., 2002).

This manuscript assesses the seasonal trends and relationships observed between, on one side, chlorophyll fluorescence, narrow-band indicators of physiological status and structural indices obtained from high-resolution hyperspectral imagery and, on the other side, GPP data measured with an eddy covariance system over an olive orchard. The vegetation dynamics around the eddy covariance tower were assessed between summer and autumn by studying the seasonal variation of chlorophyll fluorescence and reflectance indices sensitive to chlorophyll content, photosynthetic efficiency, and canopy structure calculated from pure vegetation pixels extracted from airborne hyperspectral imagery. The main hypothesis of this study was that short-term seasonal variation of GPP in an evergreen canopy would be captured adequately by physiological narrow-band remote sensing indices (i.e., below 10 nm FWHM), while indices mostly linked to canopy structure would be less sensitive.

## 2. Materials and methods

### 2.1. Study site description

The experiment was performed in a 21.5 ha olive orchard (*Olea europaea* L. cv. “Arbequina”) in “La Harina” farm located in Cordoba, Spain (37° 44' N, 4° 36' W, altitude 170 m) from summer to autumn of 2011 (DOY = 172–304). The orchard had been planted in 2005, with 4 × 1.5 m spacing. The soil was classified as a Xerofluvent (USDA Soil Taxonomy classification) and the climate was Mediterranean, with 600 mm of average annual rainfall and around 1400 mm of average annual reference evapotranspiration. The orchard was drip-irrigated twice a week for 7 h with two emitters per tree (total discharge rate: 4.4 l h<sup>-1</sup> tree<sup>-1</sup>). During the experiment, the height of the canopy was 3 m and the soil was bare after mowing the weeds in spring.

### 2.2. Eddy covariance measurements

An eddy covariance system was installed atop a mast (EC tower) near the center of the orchard (Fig. 1). It took continuous measurements from 21 June 2011 until 31 October 2011 (DOY = 172–304) and consisted of a three-dimensional sonic anemometer (model CSAT3, Campbell Scientific Inc., Logan, Utah, USA) and an open path CO<sub>2</sub>/H<sub>2</sub>O analyzer (model LI7500, LI-COR Biosciences, Lincoln, Nebraska, USA). Both sensors were placed 6 m above the ground with 20 cm of horizontal separation. Measurements of air temperature and relative humidity were taken close to the anemometer with a combined probe (model HMP45C, Vaisala, Helsinki, Finland). All the sensors were connected to a data logger (model CR1000, Campbell Scientific Inc., Logan, Utah, USA) that recorded the measurements with a sampling rate of 10 Hz. CO<sub>2</sub> concentration was measured at two heights (0.3 and 3.0 m) with a closed-path CO<sub>2</sub> analyzer (model LI-820, LI-COR Biosciences, Lincoln, Nebraska, USA) during the night to calculate CO<sub>2</sub> storage. Soil temperature was measured 7.5 cm below the surface using type K thermocouples.

The eddy covariance technique calculates the net CO<sub>2</sub> ecosystem exchange (NEE, μmol CO<sub>2</sub> m<sup>-2</sup> s<sup>-1</sup>) from the covariance between vertical wind velocity and CO<sub>2</sub> mixing ratio (Baldocchi, 2003). During nighttime, the NEE is equal to the ecosystem respiration (R<sub>eco</sub>, μmol CO<sub>2</sub> m<sup>-2</sup> s<sup>-1</sup>). The raw data were processed using Turbulent Knight 3 software (Mauder & Foken, 2011) to calculate the NEE for 30-minute periods. After this, the NEE was corrected for CO<sub>2</sub> storage based on the profile measurements. Three filters were applied to reject measurements under conditions unsuitable for the eddy covariance technique. Two filters corresponded to turbulence development and stationarity proposed by Foken et al. (2004), with a threshold of 30%, while the third used the footprint function described by Kormann and Meixner (2001). If more than 20% of the flux was generated outside the orchard, the flux was rejected, as recommended by Gockede et al.

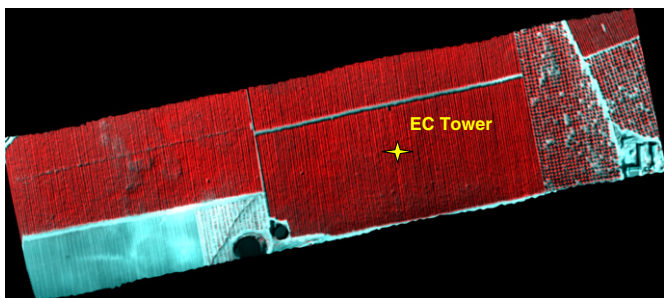


Fig. 1. Hyperspectral flightline acquired in the solar plane by the micro-hyperspectral imager on board the unmanned aerial vehicle with an IFOV of 0.93 mrad and an angular FOV of 49.82°, yielding 30 cm pixel resolution at 330 m AGL altitude. The location of the eddy covariance (EC) tower is indicated.

(2008). The use of the three filters resulted in the rejection of 69% of nighttime fluxes and 17% of daytime fluxes.

Gross primary production (GPP, μmol CO<sub>2</sub> m<sup>-2</sup> s<sup>-1</sup>) was determined as the sum of the NEE measured during daytime and R<sub>eco</sub>, extrapolated from the nighttime measurements (i.e., GPP = NEE + R<sub>eco</sub>) using a model that described the variation of R<sub>eco</sub> during the experiment. Ecosystem respiration may change over time due to changes in root biomass, in the composition of soil biota, or in soil water content. Richardson et al. (2008) proposed a model based on a first-order Fourier series to describe the variation of respiration depending on the day of year. Within each day, respiration increases non-linearly with temperature, as described by the “Q<sub>10</sub>” function, resulting in Eq. (1).

$$R_{eco} = (\beta_1 + \beta_2 \sin D + \beta_3 \cos D) Q_{10}^{(T-20)/10} \quad (1)$$

where D = DOY π/365, DOY is the day of the year and T is the temperature (°C) of the soil. β<sub>1</sub>, β<sub>2</sub>, β<sub>3</sub>, and Q<sub>10</sub> are empirical parameters that were determined by minimizing the squares of the residuals between the model and the data. The analysis started by using a global optimization with the simulated annealing algorithm and logarithmic cooling schedule (Bélisle, 1992). Based on the global optimization solution, a local optimization followed using the Nelder–Mead algorithm (Press et al., 2007). All the calculations were performed using the “bbmle” package in the R programming language (Bolker & R Development Core Team, 2012). The optimal value of the parameters and their standard errors was β<sub>1</sub> = 3.76 (0.17), β<sub>2</sub> = 1.36 (0.16), β<sub>3</sub> = 0.68 (0.21), and Q<sub>10</sub> = 1.43 (0.11), with a root mean square error of 0.91 μmol CO<sub>2</sub> m<sup>-2</sup> s<sup>-1</sup>. Fig. 2 shows diurnal GPP and NEE values measured for DOY = 242, which coincided with one of the airborne flights conducted over the site.

### 2.3. Airborne campaigns

The airborne campaigns were conducted in 2011 using a micro-hyperspectral imager on board two unmanned aerial vehicles (UAVs) operated by the Laboratory for Research Methods in Quantitative Remote Sensing, Consejo Superior de Investigaciones Científicas (QuantaLab, IAS-CSIC, Spain) (Berni et al., 2009; Zarco-Tejada et al., 2012). Two UAV platforms of different size, wingspan, and payload capacity were used over the course of the experiments, depending on the endurance required to fly over the study sites. The first UAV platform operated was

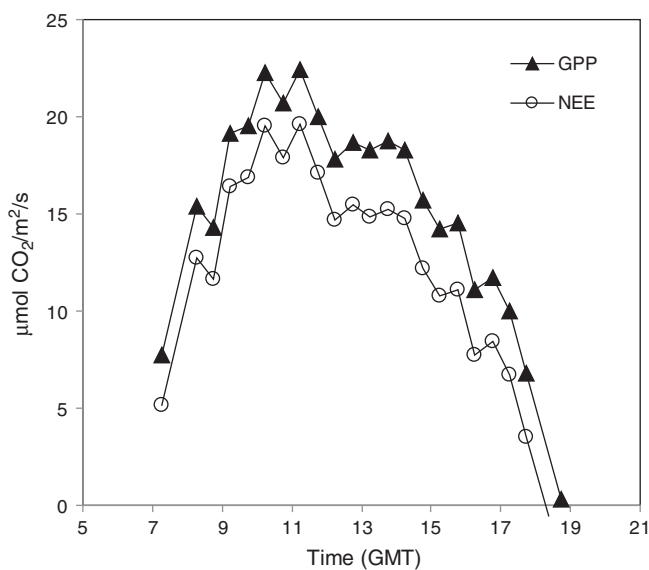


Fig. 2. GPP and NEE data measured in the olive orchard on one of the flight dates (30 August 2011).

a 2-m wingspan fixed-wing platform with up to 1-hour endurance at 5.8 kg take-off weight (TOW) and 20-minute endurance at 6.3 kg TOW (mX-SIGHT, UAV Services and Systems, Germany). A second larger UAV platform consisted of a 5-m wingspan fixed-wing platform with up to 3-hour endurance at 13.5 kg TOW (Viewer, ELIMCO, Seville, Spain). This larger platform enabled data acquisition with a larger payload, including a micro-hyperspectral imager and a thermal camera concurrently.

The platforms were controlled by an autopilot for autonomous operation (AP04, UAV Navigation, Madrid, Spain) with a dual CPU controlling an integrated Attitude Heading Reference System (AHRS) based on a L1 GPS board, 3-axis accelerometers, gyros, and a 3-axis magnetometer (Berni et al., 2009). The ground control station and the UAV were radio linked, transmitting position, attitude, and status data at 20 Hz frequency. This tunneling transmission link was used to operate the hyperspectral imager from the ground station deployed at the study site.

The hyperspectral sensor flown was the VNIR micro-hyperspectral imager (Micro-Hyperspec VNIR model, Headwall Photonics, MA, USA) configured in the spectral mode of 260 bands at 1.85 nm/pixel, 12-bit radiometric resolution and a signal-to-noise ratio (SNR) of 300:1 without binning. It yielded a full width at half maximum (FWHM) of 6.4 nm with a 25-micron slit in the 400–885 nm region. The storage rate on board the UAV was 50 fps (frames per second) with an integration time of 18 ms. The 8-mm focal length lens yielded an instantaneous field of view (IFOV) of 0.93 mrad and an angular field of view (FOV) of 49.82°, providing a swath of 317 m at 31 × 33 cm pixel resolution (resampled to 30 cm) at 330 m AGL altitude and 75 km/h ground speed (Fig. 1). The micro-hyperspectral sensor was radiometrically calibrated in the laboratory using derived coefficients with a calibrated uniform light source (integrating sphere, CSTM-USS-2000C Uniform Source System, LabSphere, NH, USA) at four levels of illumination and six integration times. Ortho-rectification of the hyperspectral imagery acquired with the UAV platforms was conducted using PARGE (ReSe Applications Schläpfer, Wil, Switzerland). This was done using input data acquired with a miniaturized inertial measuring unit (IMU) (MTiG model, Xsens, The Netherlands) installed on board and synchronized with the micro-hyperspectral imager (as shown in Zarco-Tejada et al., 2012).

In total, seven airborne campaigns were conducted over the olive orchard between DOY = 209 and DOY = 293, flying in the solar plane at a time between 8:00 and 9:00 GMT in all the campaigns except for one conducted at 7:30 GMT (Table 1). The flight plan was designed to overfly the site on each flight date. For each flightline acquired over the site, a subset of the area surrounding the EC system was created (Fig. 3) and the radiance spectra extracted.

The high-resolution hyperspectral imagery acquired (30 cm pixel size) (Fig. 3a) enabled the identification of pure vegetation pixels, removing any shadow or background effects on canopy radiance and reflectance. The selection of pure vegetation pixels was conducted using automatic object-based tree crown detection algorithms (Fig. 3b). Such algorithms successfully separated tree crowns from shaded and

sunlit soil components, obtaining pure crown radiance with and without shadow and soil effects (Fig. 3c). As seen in the figure, shadows and background affect the canopy radiance extracted from the imagery due to the aggregation of the scene components in this type of row-structured discontinuous canopies. Pure-vegetation mean radiance spectra acquired around the EC tower for each date (Fig. 4a) were used to quantify fluorescence on each date using the O<sub>2</sub>-A *in-filling* method. A total of 13 spectral bands were identified within the O<sub>2</sub>-A feature with the airborne micro-hyperspectral imager (Fig. 4b), observing the change in the depth of the oxygen feature over the course of the experiment. In addition, canopy reflectance obtained from the radiance spectra was used to calculate narrow-band vegetation indices as described in the next section.

#### 2.4. Airborne fluorescence quantification and hyperspectral index calculation

Total incoming irradiance was measured at the time of the flights using a 0.065 nm full-width half-maximum (FWHM) Ocean Optics HR2000 fiber-optic spectrometer (Ocean Optics, Dunedin, FL, USA) and a CC-3 VIS-NIR cosine corrector-diffuser as shown in Pérez-Priego et al. (2005). The instrument was calibrated in the laboratory using a LS-1-CAL calibrated tungsten halogen NIST-traceable light source (Ocean Optics, Dunedin, FL, USA). To avoid ambient temperature effects on the spectrometer, a Peltier thermally insulated box (model PT-100, Magapor, Zaragoza, Spain) was used to house the spectrometer, keeping the internal temperature stable at 24 °C ± 1 °C during field measurements. Concurrently with the sub-nanometer HR2000 spectrometer measurements acquired in the 680–770 nm range, an ASD Field Spectrometer (FieldSpec Handheld Pro, ASD Inc., CO, USA) with a cosine corrector-diffuser probe was used to measure irradiance for the entire 400–1000 nm spectral region at lower resolution (3 nm FWHM). In addition, aerosol optical measurements were acquired with a Microtops II sunphotometer (Solar Light, Philadelphia, USA) at the 440, 500, 675, 870, and 936 nm spectral bands (Table 1). The sun photometer was connected to a GPS (model GPS-12, Garmin, Kansas, USA) to obtain simultaneous readings of geographic location, altitude, and solar geometry at the time of the spectral acquisitions. To match the spectral resolution of the radiance imagery acquired by the hyperspectral airborne sensor, the higher resolution irradiance spectra measured in the field were resampled through Gaussian convolution.

Pure-vegetation mean radiance spectra extracted from the airborne hyperspectral imagery for the 260 spectral bands (Fig. 4) were used to quantify chlorophyll fluorescence and hyperspectral vegetation indices for each flight date. The Fraunhofer Line Depth (FLD) principle (Moya et al., 2004; Plascyk & Gabriel, 1975) calculated from a total of two (FLD2) and three bands (FLD3) using the *in* (L762 nm) and *out* bands (L750 nm; L780 nm) was applied to the hyperspectral imagery to quantify the canopy fluorescence signal. The method is suitable for the hyperspectral imagery used in this study, characterized by a large spectral oversampling (1.85 nm sampling interval) and 6.4 nm bandwidths (as shown in Zarco-Tejada et al., 2012). Damm et al. (2011) proved in a simulation study that the FLD method can retrieve the fluorescence signal when wider spectral bandwidths (i.e., 5 nm FWHM) are used along with high spectral sampling (below 2.5 nm) with instruments with a minimum of 300:1 signal-to-noise ratio. These modeling results agree with experimental fluorescence retrievals shown in Zarco-Tejada et al. (2012) and obtained with the micro-hyperspectral imager used in the present manuscript. A full review of methods to estimate the fluorescence signal using the FLD principle and various spectral fitting methods can be found in Meroni et al. (2010). In addition to chlorophyll fluorescence quantified from the canopy radiance spectra surrounding the EC tower site, narrow-band hyperspectral indices were calculated with regard to: i) chlorophyll a + b concentration; ii) epoxidation state of the xanthophyll cycle (EPS); iii) blue/green/red ratio indices; and iv) canopy structure (Table 2).

**Table 1**

Airborne hyperspectral flight dates and times and meteorological and atmospheric data measured at the time of each flight. DOY = day of year (days); SZA = solar zenith angle (°); Ta = air temperature (K); HR = relative humidity (%); P = atmospheric pressure (mbar); AOD = aerosol optical depth.

Date	DOY	Time (GMT)	SZA (°)	Ta (K)	HR (%)	P (mbar)	AOD (550 nm)
28/07/12	209	07:31	61.0	300.6	48.9	995.7	0.25
30/08/12	242	08:03	62.9	298.1	53.1	991.9	0.19
21/09/12	264	08:33	61.6	299.1	42.7	996	0.14
30/09/12	273	08:40	62.4	298.9	43.4	996.5	0.32
07/10/12	280	08:40	63.8	298.0	35.6	995.6	0.25
14/10/12	287	08:25	68.1	297.8	25.8	994.1	0.14
20/10/12	293	08:45	66.3	294.8	35.4	996	0.33

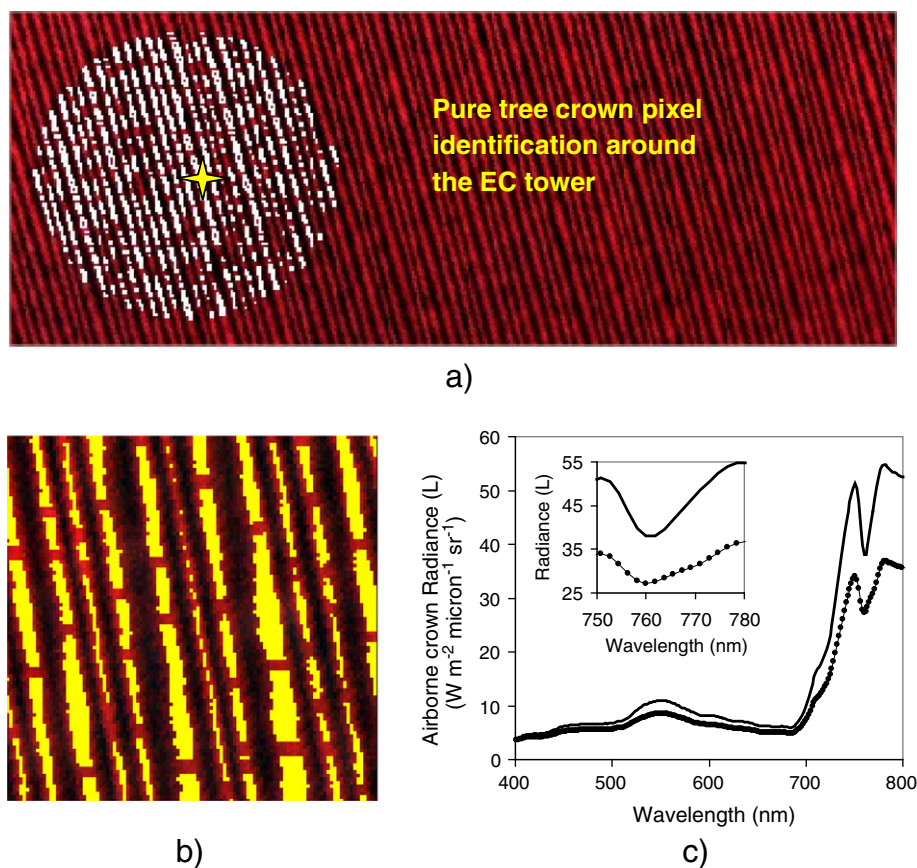


**Fig. 3.** Identification of pure vegetation pixels from the airborne hyperspectral imagery using automatic object-based detection algorithms (a,b). Mean pure radiance extracted from the area around the eddy covariance (EC) tower is shown with and without shadow and soil effects (c).

The chlorophyll a + b indices used were the Vogelmann (VOG) index (Vogelmann et al., 1993), the red edge  $R_{750}/R_{710}$  index (Zarco-Tejada et al., 2001), the family of indices based on the CARI index, such as the TCARI normalized by the OSAVI in the form suggested by Haboudane et al. (2002) (TCARI/OSAVI), and the triangular vegetation index (TVI) (Broge & Leblanc, 2000). The xanthophyll pigment indices used were the photochemical reflectance index (PRI) ( $PRI_{570}$ ) (Gamon et al., 1992) and the formulation that uses the 515 nm band as a reference ( $PRI_{515}$ ) to minimize structural effects (Hernández-Clemente et al., 2011). The blue/green/red ratio indices used were the Greenness index G and the blue/green indices BGI1 and BGI2 (Zarco-Tejada et al., 2005, 2012). Indices sensitive to canopy structure generally used for the global monitoring of vegetation canopies were calculated to assess whether changes in the tree crown structure could be captured by the NDVI (Rouse et al., 1974), the RDVI (Rougean & Breon, 1995), the enhanced vegetation index (EVI) (Huete et al., 2002), the modified triangular vegetation index (MTVI1), or the modified CARI2 index MCARI2 (see Haboudane et al., 2004, for a complete review of structural indices developed for robust estimation of LAI in crops).

In addition to the assessment of the seasonal variation of indices sensitive to physiology and structure, leaf chlorophyll concentration was estimated from airborne hyperspectral imagery on each flight date. The image-based TCARI/OSAVI and NDVI time series were used to estimate the tree crown projected leaf area index ( $LAI_p$ ) and chlorophyll content ( $C_{ab}$ ) at the tree level using the equations published in Gómez et al. (2011) and Zarco-Tejada et al. (2004), which were specifically derived for olive orchards. The calculated tree-level chlorophyll concentration, tree crown projected leaf area index, and chlorophyll fluorescence were used to explore spatial heterogeneity over time around the EC tower. The coefficient of variation (CV) was calculated using the mean ( $\mu$ ) and standard deviation ( $\sigma$ ) of

the parameters calculated from each pure-tree spectrum without shadow and soil contributions ( $CV = \sigma/\mu$ ). The temporal variation of the CV around the EC tower enabled the generation of maps showing the spatial variability of the biophysical and physiological parameters.

### 3. Results

#### 3.1. Relationships between GPP, fluorescence, and narrow-band physiological indices

The analysis of the half-hourly GPP data shows that the hyperspectral data were acquired at a time of rapid increase in the morning that reached its peak around 10.00 GMT (Fig. 5). Due to the large variability of diurnal ambient conditions throughout the experiment, which included summer and autumn dates, flux data measured at the time of the airborne flights (morning, see Table 1) did not show similar patterns when compared to flux data measured at midday (Fig. 6). In particular, the GPP data acquired at the time of the flights (between 8.00 and 9.00 GMT) showed stable values throughout the summer ( $GPP = 12\text{--}13 \mu\text{mol CO}_2/\text{m}^2/\text{s}$ ) but increased considerably after 30 September (DOY = 273) ( $GPP = 14.9 \mu\text{mol CO}_2/\text{m}^2/\text{s}$ ) and remained stable on the last three flight dates in the range of  $14\text{--}15 \mu\text{mol CO}_2/\text{m}^2/\text{s}$ . In addition, GPP measured at midday on the same flight dates showed greater variability during the summer months (GPP in the range of  $11.5\text{--}13.9 \mu\text{mol CO}_2/\text{m}^2/\text{s}$ ). Yet, coincidentally with the morning measurements, GPP reached higher values on DOY = 280 as well (GPP increased from 12 to  $14.8 \mu\text{mol CO}_2/\text{m}^2/\text{s}$  between DOY = 273 and DOY = 280). Nevertheless, midday GPP decreased at the end of the experiment (from 14.5 to  $10.4 \mu\text{mol CO}_2/\text{m}^2/\text{s}$ ) on the last two flight dates. The comparison between morning and midday GPP data measured on the flight dates shows a large diurnal

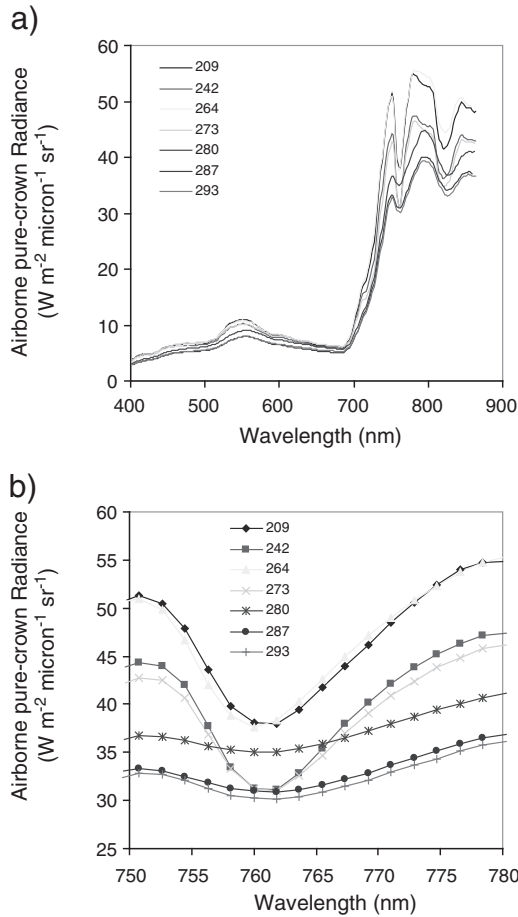


**Fig. 4.** Mean radiance spectra extracted from the airborne hyperspectral imagery around the tower flux on each flight date. Imagery acquired at 260 bands, 1.85 nm/pixel, 12-bit radiometric resolution, and 6.4 nm FWHM in the 400–885 nm region (a) showing the 13 spectral bands acquired within the O<sub>2</sub>-A feature used for fluorescence quantification (b).

variability between morning and midday. This observation is critical as it has implications for the assessment of the relationship between seasonal trends of flux data and short-term sensitive physiological indices extracted from airborne hyperspectral imagery.

The seasonal variation of O<sub>2</sub>-A depth found in both atmospheric irradiance  $E_{762\text{depth}}$  (calculated as  $E_{762}-E_{750}$ ) and canopy radiance  $L_{762\text{depth}}$  (calculated as  $L_{762}-L_{750}$ ) showed that the O<sub>2</sub>-A depth reduction observed in the airborne imagery agreed with the irradiance data measured concurrently (Fig. 7). In particular, the absolute radiance values calculated between the *in* (762 nm) and *out* (750 nm) bands over the course of the experiment showed a decrease in the O<sub>2</sub>-A band depth after DOY = 273. This was similar in both radiance and irradiance data but inversely related to the morning GPP increase measured at the same time (Fig. 6). Both radiance and irradiance O<sub>2</sub>-A band depths decreased at the end of summer, although the changes in irradiance depth at 760 nm occurred earlier than the decrease observed in radiance *in-filling*. These changes in O<sub>2</sub>-A depth cannot be attributed solely to variations in solar zenith angle and aerosol optical depth throughout the season as the major drivers (see Table 1). They are also due to the contribution of the chlorophyll fluorescence signal *in-filling* to the O<sub>2</sub>-A feature.

An overall assessment of the relationships between GPP and the narrow-band airborne indices is shown in Table 3. As regards the indices most sensitive to canopy structure (such as the NDVI and the EVI, among others), non-significant relationships were found with morning GPP ( $r^2 = 0.17$ ;  $p > 0.05$ ). The seasonal variation of the three physiological indices related to chlorophyll content, that is, the TCARI/OSAVI (shown as OSAVI/TCARI for a direct relationship with GPP, Fig. 8a), light use efficiency, the PRI<sub>570</sub> (Fig. 8b), and chlorophyll fluorescence, FLD3 (Fig. 8c) showed a close trend when compared with the morning GPP measured at the same time of the flights. By contrast, neither the NDVI nor the EVI changed throughout the season (NDVI shown in Fig. 8d). The NDVI yielded better results than the EVI when compared to GPP. The trend observed for GPP and the indices linked to physiology and structure (Fig. 8) was captured by the chlorophyll index TCARI/OSAVI ( $r^2 = 0.75$ ;  $p < 0.05$ ), PRI<sub>570</sub> ( $r^2 = 0.75$ ;  $p < 0.05$ ) and the fluorescence signal quantified with the FLD3 method ( $r^2 = 0.8$ ;  $p < 0.05$ ). As mentioned, the NDVI showed a non-significant relationship with morning GPP ( $r^2 = 0.17$ ;  $p > 0.05$ ), as opposed to the physiological indices.

**Table 2**  
Narrow-band hyperspectral optical indices used in this study.

Index	Equation	Reference
<b>Chlorophyll indices</b>		
Vogelmann (VOG)	$VOG = R_{740}/R_{720}$	Vogelmann et al. (1993)
Red edge R750/R710	$R_{750}/R_{710}$	Zarco-Tejada et al. (2001)
TCARI	$TCARI = 3 * [(R_{700} - R_{670}) - 0.2 * (R_{700} - R_{550}) * (R_{700}/R_{670})]$	Haboudane et al. (2002)
TCARI/OSAVI	$TCARI/OSAVI = [3 * [(R_{700} - R_{670}) - 0.2 * (R_{700} - R_{550}) * (R_{700}/R_{670})]] / [(1 + 0.16) * (R_{800} - R_{670}) / (R_{800} + R_{670} + 0.16)]$	Haboudane et al. (2002)
TVI	$TVI = 0.5 * [120 * (R_{750} - R_{550}) - 200 * (R_{670} - R_{550})]$	Broge and Leblanc (2000)
<b>Xanthophyll indices</b>		
PRI <sub>570</sub>	$PRI_{570} = (R_{570} - R_{531}) / (R_{570} + R_{531})$	Gamon et al. (1992)
PRI <sub>570</sub>	$PRI_{570} = (R_{515} - R_{531}) / (R_{515} + R_{531})$	Hernández-Clemente et al. (2011)
<b>Blue/green/red ratio indices</b>		
G	$G = R_{550} / R_{670}$	–
BGI1	$BGI_1 = R_{400} / R_{550}$	Zarco-Tejada et al. (2005, 2012)
BGI2	$BGI_2 = R_{450} / R_{550}$	–
<b>Structural indices</b>		
NDVI	$NDVI = (R_{800} - R_{670}) / (R_{800} + R_{670})$	Rouse et al. (1974)
RDVI	$RDVI = (R_{800} - R_{670}) / (R_{800} + R_{670})^{0.5}$	Rougean and Breon (1995)
EVI	$EVI = 2.5 * (R_{800} - R_{670}) / (R_{800} + 6 * R_{670} - 7.5 * R_{400} + 1)$	Huete et al. (2002)
MTVI1	$MTVI1 = 1.2 * [1.2 * (R_{800} - R_{550}) - 2.5 * (R_{670} - R_{550})]$	Based on Broge & Leblanc (2000) and Haboudane et al. (2004)
MCARI2	$MCARI2 = \frac{1.5 * [2.5 * (R_{800} - R_{670}) - 1.3 * (R_{800} - R_{550})]}{\sqrt{(2 * R_{800} + 1)^2 - (6 * R_{800} - 5 * \sqrt{R_{670}}) - 0.5}}$	Haboudane et al. (2004)
<b>Fluorescence retrieval</b>		
FLD2 (750; 762)	FLD method using 1 reference band	Plascyk and Gabriel (1975), Moya et al. (2004)
FLD3 (750; 762; 780)	FLD method using 2 reference bands	–

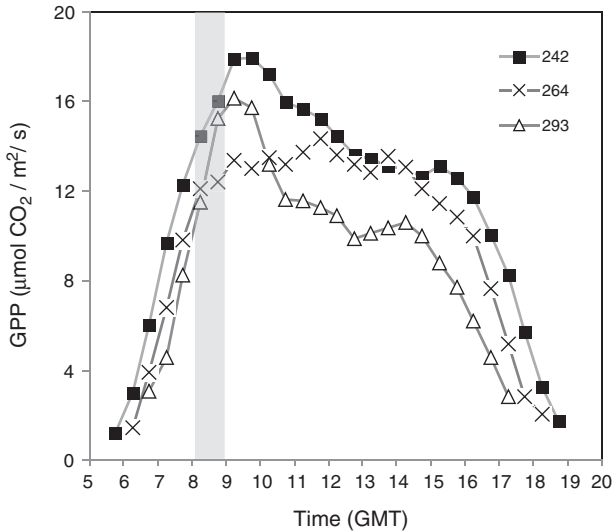


Fig. 5. Diurnal GPP data measured on selected dates when the airborne hyperspectral flights were conducted. The shaded band shows the time of the flights.

Results obtained for the seasonal variation of the narrow-band physiological indices are in agreement with the seasonal variation observed in leaf chlorophyll content estimated from hyperspectral imagery over the course of the experiment. In particular, chlorophyll content estimated from the TCARI/OSAVI increased between summer (end of July) and autumn (end of October) from 60.9 to 71.8 µg/cm<sup>2</sup> (17.9% variation), while LAI<sub>p</sub> estimated from NDVI remained constant over the season with variations below 0.15 units of LAI<sub>p</sub> (3%) (LAI<sub>p</sub> ranged from 4.77 to 4.62 throughout the experiment) (Fig. 9). These changes in chlorophyll and crown structure over the season were not significantly related ( $r^2 = 0.31$ ;  $p > 0.05$ ). This proves the different sensitivity of both indices to biophysical and biochemical (chlorophyll content) seasonal variation obtained from hyperspectral imagery. These results show the small seasonal structural changes throughout the season in the orchard canopy under study.

### 3.2. Temporal relationships between narrow-band indices

Seasonal relationships between narrow-band indices calculated from the hyperspectral imagery acquired over the flux tower site are shown in Table 4. Overall and as expected, the relationships

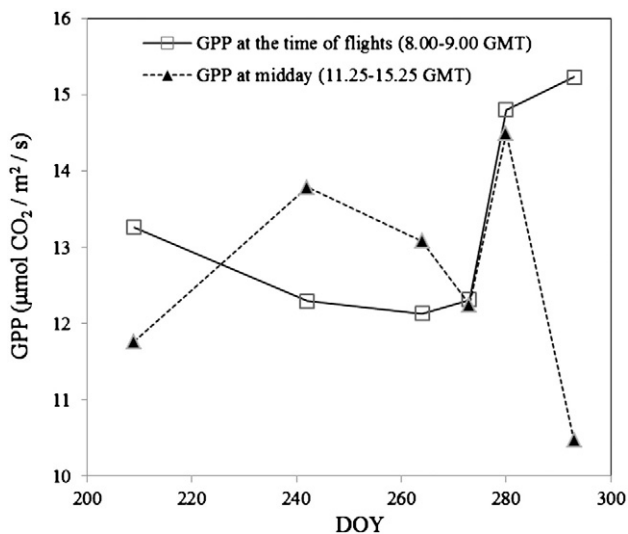


Fig. 6. GPP acquired between 11:25 and 15:25 GMT and at the time of each flight.

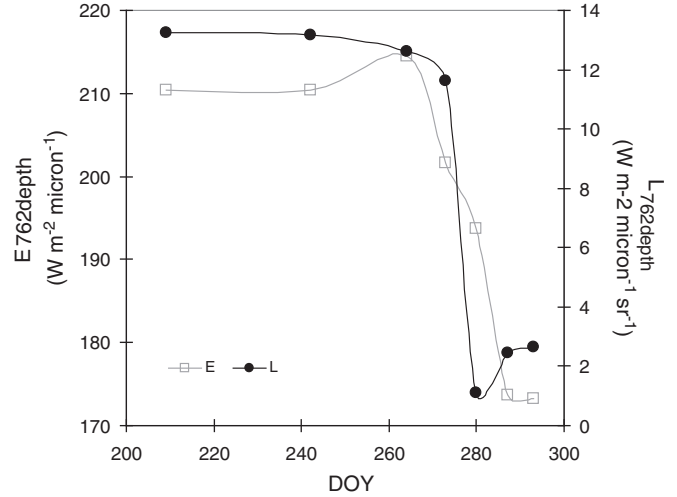


Fig. 7. Depth of atmospheric irradiance ( $E_{762depth}$ ) and canopy radiance ( $L_{762depth}$ ) measured throughout the season in the O<sub>2</sub>-A spectral feature.

obtained between indices of the same functional group were statistically significant. In other words, the chlorophyll indices used in this study were well related to each other ( $p < 0.001$  in all cases), except for the R<sub>750</sub>/R<sub>710</sub> index, which did not relate well over time with the VOG, TCARI/OSAVI, or TVI indices. Similar results were found for the structural indices, which were all well related within the same group of structural indices ( $p < 0.001$  in most cases).

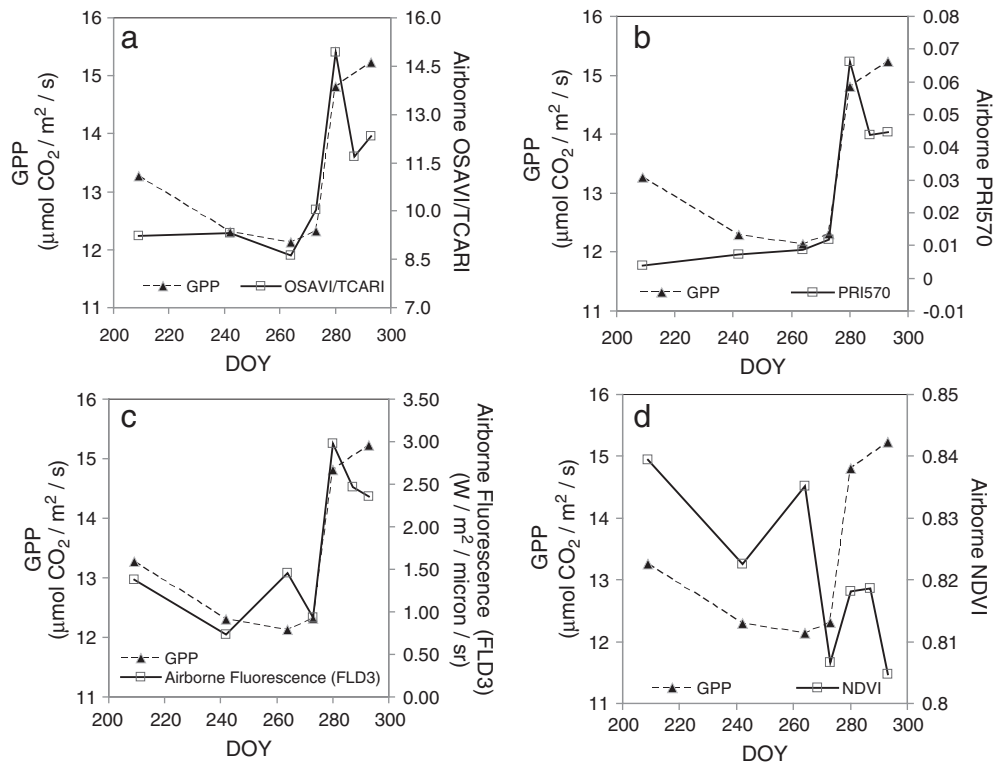
Results shown in Table 4 demonstrate that the small structural changes that occurred throughout the season yielded weak or no relationships with physiological changes captured by indices sensitive to chlorophyll a + b (such as the TCARI/OSAVI), light use efficiency (PRI indices), and fluorescence signal emission (FLD2, FLD3). In all these cases, the indices sensitive to structural changes did not yield significant relationships with the physiological indices ( $p > 0.05$ ) and showed relationships only with the VOG and the TVI ( $p < 0.05$ ), and the blue/green/red ratio indices G, BG11 ( $p < 0.05$ ), and BG12

Table 3

Coefficients of determination ( $r^2$ ) and statistical significance (p-values) for GPP compared with chlorophyll, physiological, blue/green/red ratio, and structural indices and chlorophyll fluorescence extracted from pure vegetation pixels surrounding the EC tower.

Index	GPP
Chlorophyll indices	
Vogelmann (VOG)	0.49
R750/R710	0.49
TCARI	<b>0.68*</b>
TCARI/OSAVI	<b>0.76*</b>
TVI	0.42
Xanthophyll indices	
PRI <sub>570</sub>	<b>0.75*</b>
PRI <sub>515</sub>	0.01
Blue/green/red ratio indices	
G	0.51
BG11	0.20
BG12	0.26
Structural indices	
NDVI	0.17
RDVI	0.01
EVI	0.01
MTVI1	0.01
MCARI2	0.01
Fluorescence retrieval	
FLD2 (750; 762)	<b>0.74*</b>
FLD3 (750; 762; 780)	<b>0.80*</b>

\*  $p < 0.05$ .



**Fig. 8.** Seasonal variation of the physiological indices related to (a) chlorophyll content (TCARI/OSAVI, shown as OSAVI/TCARI), (b) photosynthetic efficiency (PRI<sub>570</sub>), (c) chlorophyll fluorescence quantified by the FLD3 method, and d) NDVI index. The three physiological indices show a trend close to GPP measured at the same flight times.

( $p < 0.01$ ). The most robust chlorophyll index used in crop canopies (TCARI/OSAVI) showed no significant relationship with the NDVI ( $p > 0.05$ ), yielding similar results for the PRI and fluorescence quantified by FLD methods ( $p > 0.05$ ).

The physiological indices were related to each other throughout the season: the chlorophyll index TCARI/OSAVI was highly related with the PRI<sub>570</sub> ( $r = -0.97$ ;  $p < 0.001$ ) and with chlorophyll fluorescence emission quantified by the FLD3 ( $r = -0.86$ ;  $p < 0.01$ ). Fluorescence quantification (FLD2, FLD3) showed highly significant relationships with the PRI<sub>570</sub> ( $r > 0.9$  in all cases;  $p < 0.01$ ). These results suggest that small physiological changes occurring throughout the season were captured by narrow-band indices sensitive to different physiological indicators and calculated from various parts of the spectrum: the visible region

(PRI), the visible and near infrared (TCARI/OSAVI), and fluorescence quantification through the 760 nm oxygen absorption feature.

The large increase in chlorophyll content, light use efficiency, and fluorescence during the first part of October is consistent with the seasonal changes in canopy conductance of olive trees reported by Testi et al. (2006). This change was not associated to changes in water supply as no rainfall occurred during the second half of the experiment.

### 3.3. Spatio-temporal variation of LAI<sub>p</sub>, chlorophyll content, and fluorescence emission around the tower

Crown-level indices were used to calculate LAI<sub>p</sub> and chlorophyll content and fluorescence at the tree level around the tower, enabling the estimation of each parameter without shadow or background effects (Fig. 10 for fluorescence) and generating interpolated maps to show their spatial variation. This methodology made it possible to obtain continuous maps around the tower without shadow or soil effects. The spatial variation of LAI<sub>p</sub> and chlorophyll content and fluorescence showed consistent results for two dates with large GPP variation over the experiment at the end of the summer (30 Sept.) and the beginning of autumn (20 Oct.) (Fig. 11). In particular, the maps correspond to dates before and after the rapid physiological change experienced when the summer season concluded. The mean values for all trees on DOY = 273 as compared to DOY = 293 showed an almost nonexistent variation of tree-level LAI<sub>p</sub> ( $\mu = 4.63$  for DOY = 273;  $\mu = 4.62$  for DOY = 293); however, changes were found in physiological parameters such as chlorophyll content ( $\mu = 64.1 \mu\text{g}/\text{cm}^2$  for DOY = 273;  $\mu = 71.8 \mu\text{g}/\text{cm}^2$  for DOY = 293) and particularly in chlorophyll fluorescence ( $\mu = 0.93 \text{ W m}^{-2} \mu\text{m}^{-1} \text{ sr}^{-1}$  for DOY = 273;  $\mu = 2.36 \text{ W m}^{-2} \mu\text{m}^{-1} \text{ sr}^{-1}$  for DOY = 293).

The assessment of the spatial variability of the parameters showed a smaller variation in LAI<sub>p</sub> (Fig. 11, top) than in chlorophyll fluorescence and chlorophyll content (Fig. 11, middle and bottom). This visual result agreed with the quantification of the coefficient of variation (CV) for all dates (Fig. 12), which showed that the

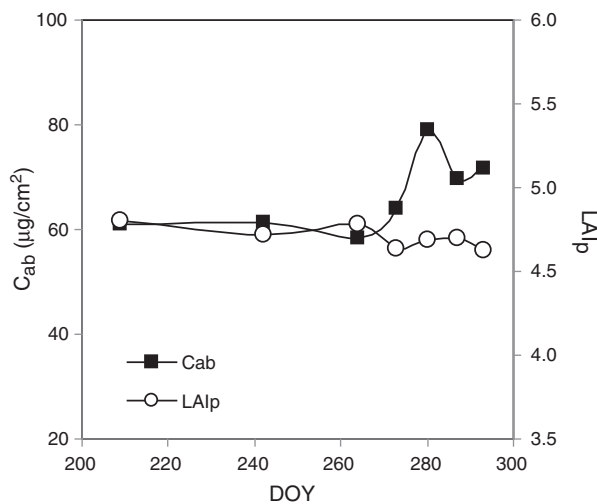


**Fig. 9.** Temporal variation of image-estimated chlorophyll ( $C_{a+b}$ ) content and tree crown-projected LAI (LAI<sub>p</sub>) calculated from the pure-tree crowns around the EC tower.

**Table 4**  
Relationships between narrow-band hyperspectral indices calculated from the time-series airborne imagery acquired over the EC tower site.

		Chlorophyll indices					Xanthophyll indices		B / G Ratio Indices			Structural indices					Fluorescence indices	
		VOG	R750 / R710	TCARI	TCARI / OSAVI	TVI	PRI 570	PRI 515	G	BGI1	BGI2	NDVI	RDVI	EVI	MTVI1	MCARI2	FLD2	FLD3
Chlorophyll indices	VOG	1																
	R750 / R710	-0.37	1															
	TCARI	0.97***	-0.52	1														
	TCARI/OSAVI	0.93**	-0.64	0.99***	1													
	TVI	0.94**	-0.21	0.93**	0.88**	1												
Xant. ind.	PRI570	-0.84*	0.70	-0.94**	-0.97***	-0.84*	1											
	PRI515	-0.59	-0.17	-0.46	-0.38	-0.53	0.27	1										
B / G indices	G	0.88**	-0.37	0.91**	0.89**	0.92**	-0.89**	-0.61	1									
	BGI1	-0.63	-0.20	-0.59	-0.50	-0.69	0.35	0.49	-0.53	1								
	BGI2	-0.74	-0.08	-0.71	-0.63	-0.81*	0.54	0.72	-0.79*	0.90**	1							
Structural indices	NDVI	0.78*	0.18	0.69	0.60	0.83*	-0.49	-0.81	0.79*	-0.82*	-0.94**	1						
	RDVI	0.59	0.52	0.44	0.31	0.68	-0.18	-0.60	0.46	-0.75	-0.71	0.85*	1					
	EVI	0.58	0.48	0.42	0.00	0.68	-0.21	-0.56	0.47	-0.57	-0.58	0.77*	0.96***	1				
	MTVI1	0.60	0.50	0.46	0.33	0.70	-0.20	-0.55	0.46	-0.72	-0.68	0.82*	0.99***	0.97***	1			
	MCARI2	0.63	0.48	0.47	0.34	0.70	-0.22	-0.64	0.50	-0.69	-0.69	0.85*	0.99***	0.98***	0.99***	1		
Fluor. indices	FLD2	-0.61	0.88**	-0.77*	-0.84*	-0.58	0.93**	0.07	-0.73	0.09	0.31	-0.20	0.20	0.16	0.17	0.16	1	
	FLD3	-0.63	0.85*	-0.79*	-0.86*	-0.61	0.94**	0.08	-0.76*	0.16	0.36	-0.24	0.15	0.13	0.13	0.12	0.99***	1

\* p<0.05; \*\* p<0.01; \*\*\* p<0.001.

Relationships obtained for p<0.05 or better among the different functional groups of indices are shaded.

fluorescence signal around the tower varied by 17% in summer while LAI<sub>p</sub> was little affected (CV = 1.8%). The temporal variation of CV for all dates showed that, after the summer stress period, chlorophyll fluorescence greatly decreased from CV = 17% in summer to CV = 9% in autumn; LAI<sub>p</sub> remained constant in that period (CV ranged from 1.5% to 2% between summer and autumn). The trend observed in chlorophyll content variability around the EC tower during the same period yielded a CV between 13% and 7%. In the same trees, the analysis revealed a declining trend in the CV of chlorophyll content and fluorescence around the end of summer, and a higher CV of chlorophyll fluorescence than chlorophyll content at the time of the maximum stress during summer. At the end of the experiment in autumn, with milder ambient conditions, the CV of both chlorophyll content and fluorescence reached closer values (8–9%). The higher CV obtained for fluorescence and chlorophyll than for the structural parameter showed the greater spatio-temporal dynamics of the physiological indices. The maps shown in Fig. 11 and the spatio-temporal analysis conducted suggest that pixels with similar canopy densities may contain different levels of chlorophyll content and fluorescence emission, contributing differently to the carbon fluxes measured by the EC tower.

**4. Discussion**

In this study we assessed the seasonal trends of GPP, chlorophyll fluorescence, and narrow-band physiological indices acquired with airborne hyperspectral imagery on seven dates over an orchard instrumented with eddy covariance throughout summer and autumn. The study made it possible to draw conclusions regarding the spatio-temporal variability and sensitivity of physiological and structural indices to short-term seasonal changes. Moreover, it raises new questions concerning the accurate assessment of the dynamics of CO<sub>2</sub>

exchange in non-homogeneous canopies. In particular, the crop under study was an evergreen canopy, characterized by small seasonal structural changes and a stable leaf area. The high spatial resolution imagery was acquired at 30 cm pixel size and 260 spectral bands in the 400–900 spectral region. This enabled the selection of pure-vegetation crown pixels to quantify chlorophyll fluorescence through the Fraunhofer Line Depth (FLD) principle, physiological reflectance indices related to chlorophyll content, photosynthetic efficiency, and structural indices. The results obtained between GPP and the narrow-band indices acquired from the airborne hyperspectral imagery were non-significant for the indices sensitive to structure (such as the NDVI and EVI) (r<sup>2</sup> = 0.17; p > 0.05). By contrast, physiological indices related to chlorophyll content (TCARI/OSAVI), light use efficiency (PRI<sub>570</sub>), and chlorophyll fluorescence showed a close trend when compared with GPP measured at the same time (r<sup>2</sup> > 0.7; p < 0.01 for the TCARI/OSAVI, fluorescence, and PRI<sub>570</sub>). This study highlights that the NDVI and EVI showed a slower response than the physiological indices to changes in leaf pigmentation, as they are less sensitive to such physiological dynamics. For this reason, such indicators based on standard vegetation indices mostly linked to canopy structure are not good indicators of short-term (i.e., seconds to days) physiological changes in canopies with a stable structure.

During the season, chlorophyll content estimated from the imagery increased by 17.9% between summer (end of July) and autumn (end of October), while the NDVI and estimated crown LAI<sub>p</sub> remained constant within a small range of variation of 0.15 units (LAI<sub>p</sub> ranged between 4.62 and 4.77). This small variation in the NDVI may be due either to the low net growth of the canopy or to the greater sensitivity of structural indices to vertical rather than lateral canopy growth. Nevertheless, under such small seasonal variation of NDVI as an indicator of canopy growth, physiological indices and fluorescence showed a consistent behavior throughout the season, showing trends that resembled the variation of GPP.

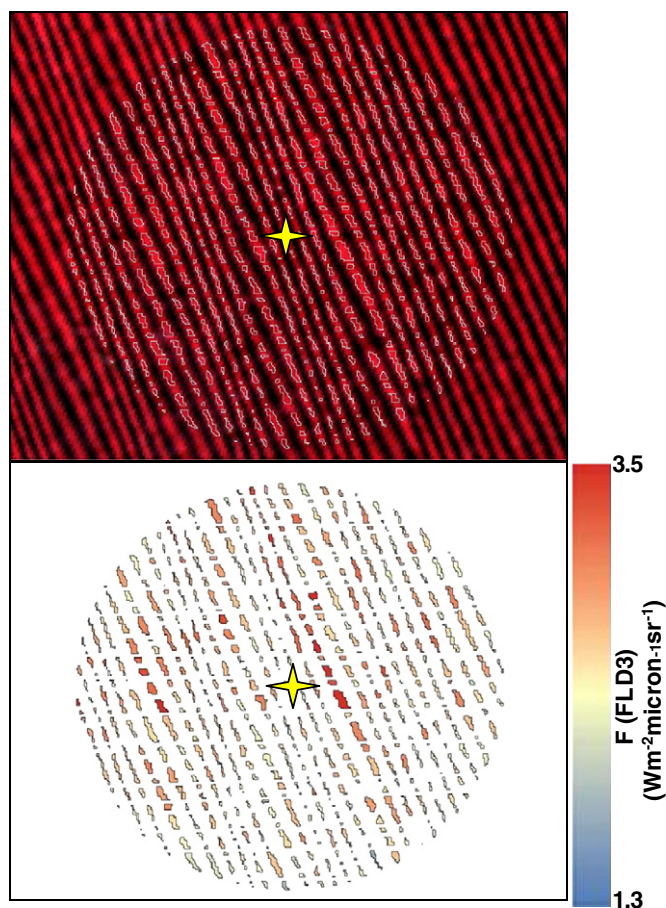


**Fig. 10.** Chlorophyll fluorescence ( $F$ ) quantified in pure tree crowns without shadow and background effects (top) using the FLD3 method (bottom) for 30 September flight date.

Among the different methods used to quantify chlorophyll fluorescence, the Fraunhofer Line Depth (FLD) principle based on three spectral bands (750 nm; 762 nm; 780 nm) yielded a slightly better performance than its use based on two bands (750 nm; 762 nm). Yet, their significance level was the same. This result agrees with those of Zarco-Tejada et al. (2012) when using the same high sampling interval (1.85 nm/pixel) and 6.4 nm bandwidth hyperspectral imager. In this study, the flights were performed in the morning (i.e., 8:00–9:00 GMT, which corresponds to 10:00–11:00 h local time in summer). This time of day was chosen instead of midday in order to avoid turbulences that would affect the airborne platform used to acquire the hyperspectral imagery. A later flight could have been more related to the midday GPP measured by the tower, avoiding the rapid changes in GPP in the morning. Yet, other studies have demonstrated that the highest differences in fluorescence between stress levels are found in the morning and that such differences among treatments decrease at midday due to the high saturating irradiance levels and temperature (Zarco-Tejada et al., 2009). This issue warrants further attention when developing the experimental setups (i.e., earlier morning flights as opposed to midday) when the aim is to monitor fluorescence as an indicator of physiological condition.

In addition, careful attention is required regarding the flight altitude and atmospheric conditions for an accurate retrieval of the fluorescence signal. In this study, the flights were always conducted at the same altitude and close to the ground (330 m AGL); in addition, atmospheric data were acquired during the flight to assess whether the fluorescence retrieval was highly affected by atmospheric changes. When working with airborne platforms for remote sensing research, flexibility of

operation enables the selection of clear-sky days for the airborne campaigns. Thus, flights are not usually conducted in hazy or cloudy conditions. The assessment conducted to find out whether the atmospheric conditions affected the retrieval of fluorescence indicated that under the conditions of this study, no relationships were found between fluorescence quantification and both aerosol optical depth ( $r^2 = 0.01$ ; n.s.) and atmospheric pressure ( $r^2 = 0.06$ ; n.s.); however, the sun angle showed a weak non-significant relationship as the sun angle changes were small during the experiment, ranging between  $61^\circ$  and  $68^\circ$  ( $r^2 = 0.35$ ; n.s.). Any potential relationships between AOD and GPP data measured by the tower were also excluded ( $p > 0.05$ ). Therefore, the experimental setup of this study, characterized by a low-altitude sensor flying over a flat area under similar atmospheric conditions, suggested that the relationships obtained were hardly affected by the small changes in the atmosphere during the airborne campaigns. Nevertheless, this issue is critical when assessing fluorescence under varying atmospheric conditions or sun angles in diurnal setups, or when retrieving fluorescence from future satellite platforms. Hence, further efforts are needed through dedicated modeling and experimental studies. Such important atmospheric effects are less critical when low altitude flights are conducted. This is the case of the present study and most assessments focusing on low-altitude flights for precision agriculture and genetic screenings.

Another important issue that requires attention is the modulation of the fluorescence signal by irradiance and the relationship between irradiance levels and GPP over the course of the day and throughout the season. In this study, the radiance and irradiance depths were calculated in the  $O_2$ -A band ( $L_{762\text{depth}}$  and  $E_{762\text{depth}}$ ). A comparison of the data with the seasonal variation of morning GPP showed that radiance depth was more significantly related to GPP than  $E_{762\text{depth}}$  (considering both the coefficient of determination and the statistical significance,  $p$ -value). As expected, GPP showed a modulation with incoming irradiance measured in the field at the time of the flights. Irradiance depth at 762 nm was related to GPP for the entire time series ( $r^2 = 0.68$ ;  $p < 0.05$ ). Yet, both the fluorescence signal quantified by FLD3 and the  $L_{762\text{depth}}$  yielded more significant results when compared to GPP (in the range of  $r^2 = 0.8$ ;  $p < 0.05$  for FLD3 and  $L_{762\text{depth}}$ ). Thus, these results show that the *in-filling* signal extracted from pure-vegetation canopy radiance was more closely related to GPP than irradiance depth calculated at 760 nm, suggesting that the statistically significant relationships obtained by the physiological indices were not driven by (although they were consistently related to) irradiance levels only.

The robustness of the hyperspectral dataset used in this study was demonstrated when assessing the relationships between the various physiological and structural indices over the season. In fact, the small structural changes in the canopy that occurred throughout the season were responsible for the absence of a relationship between the structural indices and the physiological indices sensitive to chlorophyll a + b (TCARI/OSAVI), photosynthetic efficiency (PRI indices), and the fluorescence signal emission (FLD3). In particular, the seasonal trend of the TCARI/OSAVI chlorophyll index was highly associated with the  $PRI_{570}$  and chlorophyll fluorescence emission ( $p < 0.01$ ). Moreover, chlorophyll fluorescence quantification using the FLD method showed highly statistically significant relationships with the  $PRI_{570}$  ( $p < 0.001$ ). Although the PRI obtained good results in this seasonal study, careful attention is required when using the PRI as an index to track the dynamics of epoxidation state of the xanthophyll cycle at the canopy level. The reason is that several studies have shown the very strong impact that canopy structure, illumination, shadows, observation geometry, and other leaf pigments such as chlorophyll and carotenoid content have on the PRI when calculated at the canopy level. Such structural effects were minimized in this study due to the small canopy variability throughout the season. Nevertheless, they need to be taken into account when time-series PRI data are used as a proxy for GPP in canopies with fast phenological

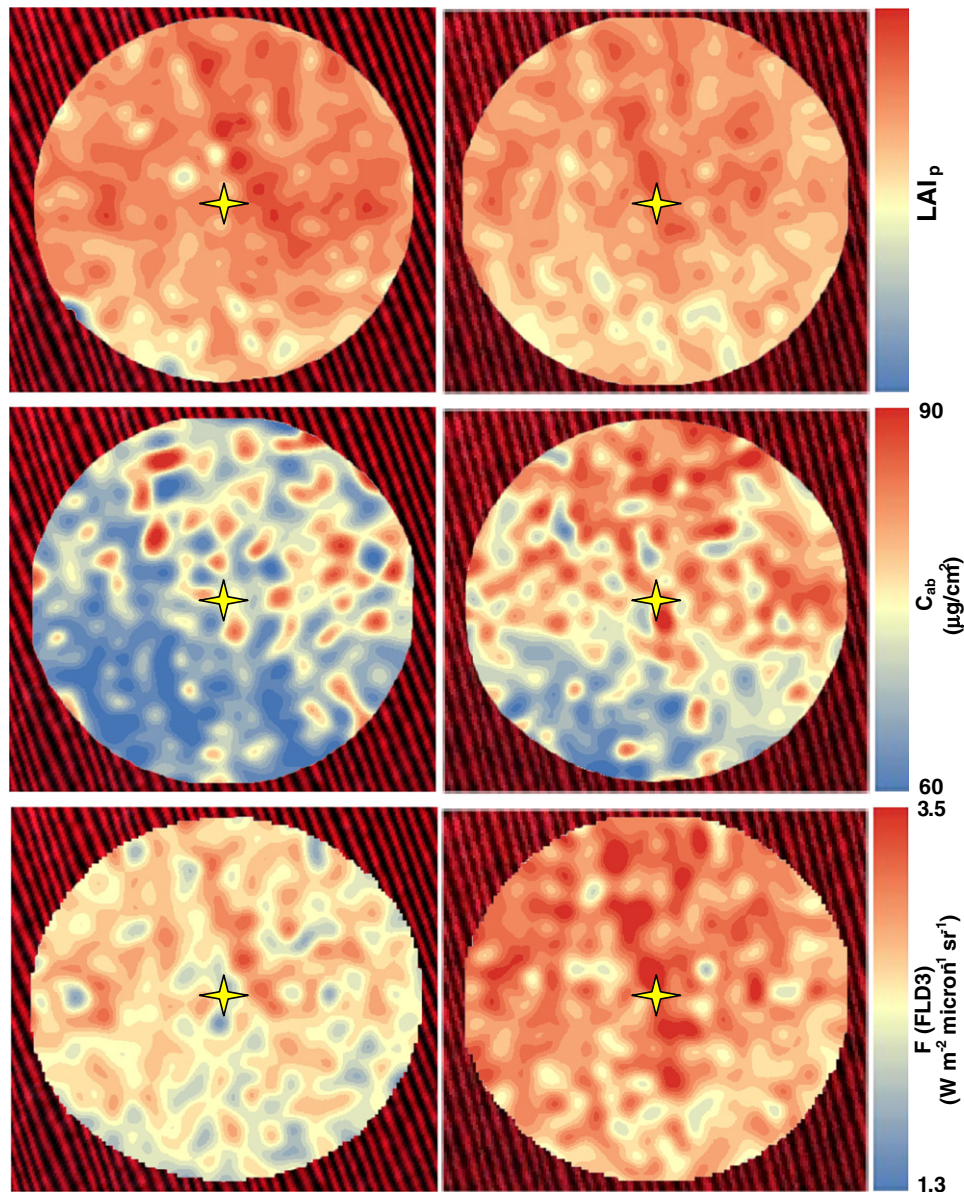


**Fig. 11.** Interpolated maps of tree crown projected LAI ( $LAI_p$ ) (top), chlorophyll content ( $C_{a+b}$ ) (middle), and chlorophyll fluorescence ( $F$ ) (bottom) calculated from single-tree spectra on flight dates showing large differences in GPP – 30 Sept. (left) and 20 Oct. (right).

changes. In such cases, the PRI may be affected by the structure as a major driver of the changes observed.

Another interesting result that requires attention is related to the spatial variability of the remote sensing physiological and structural indices as a methodology to assess vegetation stress and dynamics. This assessment can be performed using very high resolution hyperspectral imagery to enable the identification of pure vegetation pixels with low background or shadow effects. In particular, the spatio-temporal analysis conducted in this study to quantify the variability of the physiological and structural hyperspectral indices was based on the coefficient of variation, using the pure tree pixels identified around the eddy covariance tower. The temporal trend of the CV for all flight dates revealed that chlorophyll fluorescence emission around the tower varied up to 17% at the time of maximum stress in summer, while  $LAI_p$  yielded a low spatial variability during the same period ( $CV = 1.8\%$ ). Therefore, the canopy was structurally homogeneous but greater physiological variability was found when using remote sensing indices related to chlorophyll and xanthophyll pigments and fluorescence. Moreover, after the summer stress period ended, fluorescence and chlorophyll

content showed a decreasing trend in autumn, with a decrease in the CV around the tower from 17% to 9%. During the same period, the CV of the NDVI structural index and the estimated  $LAI_p$  showed a constant trend ( $CV = 1.5\%–2\%$ ). During both summer and autumn, the trees around the tower showed the highest variability in fluorescence emission, followed by chlorophyll content. In autumn, a time of low ambient stress conditions, their CV reached similar values (8–9%).

For these reasons, the results of this study demonstrate that even small physiological changes occurring in an evergreen crop canopy, characterized by small seasonal structural variation, were captured by airborne-derived narrow-band indices related to chlorophyll content, light use efficiency, and chlorophyll fluorescence. Moreover, this research suggests that physiological remote sensing indices related to photosynthetic pigments (i.e., chlorophyll and xanthophylls) and fluorescence/photosynthetic hyperspectral indices are required when the aim is to track short-term photosynthetic variation, using GPP in this study as a comparison. Results of assessing the spatial variability of the physiological indices around the tower agree with previous studies that have suggested using the variability of canopy parameters (i.e.,

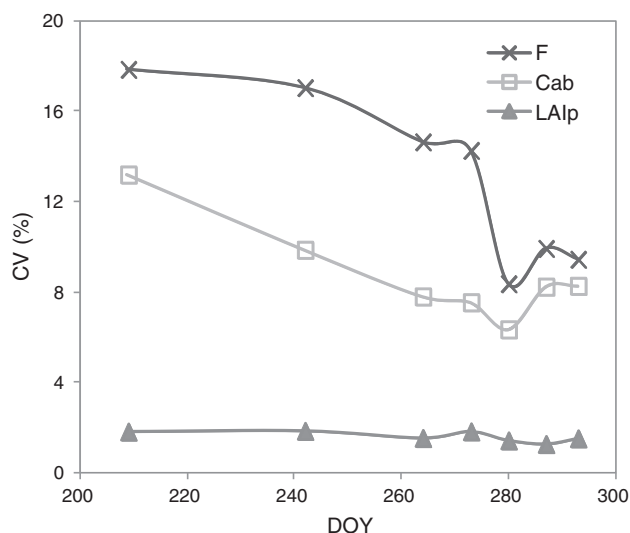


**Fig. 12.** Temporal trend of the coefficient of variation (CV) calculated for chlorophyll content ( $C_{a+b}$ ), tree crown projected LAI ( $LAI_p$ ) and chlorophyll fluorescence (F) for the trees surrounding the EC tower.

in temperature) as an indicator of physiological status (Gardner et al., 1981). These studies have shown that variability increases with stress (Fuchs, 1990) but requires high spatial resolution in the case of heterogeneous canopies (Leinonen & Jones, 2004; Moller et al., 2007). When very high-resolution data are available, successful assessment of within-tree thermal variability has proven to be an indicator of stress using 12 cm airborne thermal imagery (González-Dugo et al., 2012). A similar assessment was conducted in this experiment, although considering indicators more potentially linked to photosynthesis such as chlorophyll fluorescence and chlorophyll content. Results demonstrated a consistent behavior of within-field variability of chlorophyll fluorescence and chlorophyll content over time as a function of seasonal ambient conditions. This finding may have implications for quantifying the dynamics of  $CO_2$  exchange in trees that appear to have a homogeneous structure but show a gradient in physiological condition that can influence their photosynthetic rates.

Further studies will focus on the effects of the spatial variability of plant physiological conditions on the contribution to the dynamics of  $CO_2$  exchange as measured by the EC tower, and the spatial assessment of the actual footprint of turbulence during each flight using very high resolution imagery as shown in this study. In heterogeneous canopies with mixed species, it may be necessary to consider the variation of physiological conditions among trees combined with changes in footprint shape throughout the season when assessing relationships between spectral indices and fluxes. Additional issues that require further attention include the effects of chlorophyll fluorescence emission on the narrow bands used to calculate hyperspectral indices such as the CARI, MCARI, or TCARI family used to estimate chlorophyll content through the TCARI/OSAVI, as well as other red edge indices. The temporal dynamics of chlorophyll content estimated from the TCARI/OSAVI in this study may be partially affected by the modulation of the chlorophyll fluorescence signal, which may affect bands in the 670–750 nm spectral range. Other important issues that require further study are the potential atmospheric and scattering effects on the retrieval of fluorescence, both considering high-altitude (satellite) and low-altitude (airborne) levels. The potential effects of aerosol optical depth, flight altitude, atmospheric pressure, and sun angle need to be assessed through a modeling approach and validated with ground truth fluorescence data measured concurrently. A quantification of such effects through physical

modeling will be required as part of the efforts to understand spatio-temporal trends of physiological indices linked with stress and carbon dynamics with hyperspectral imagery.

## 5. Conclusions

This study makes progress on the assessment of the spatio-temporal trends of chlorophyll fluorescence and physiological indices quantified with hyperspectral imagery acquired over a non-homogeneous canopy characterized by small seasonal structural changes. The concurrent measurements of  $CO_2$  fluxes acquired with an eddy covariance system enabled the comparison of the net and gross primary production with physiological and structural remote sensing indices in a total of seven flights. Such flights were conducted between summer and autumn with a hyperspectral camera that captured 30 cm resolution imagery and 260 spectral bands in the 400–900 nm region, targeting pure tree crowns without shadow components or background effects. The work highlights that the seasonal physiological changes occurring in an evergreen, non-homogeneous canopy with a stable leaf area (as described by the time series of gross primary production retrieved by eddy covariance) can be captured by remote sensing physiological indices related to chlorophyll content (TCARI/OSAVI), light use efficiency (PRI) and chlorophyll fluorescence quantification. In contrast, indices associated with the structure of the canopy (i.e. NDVI, EVI) showed a very poor correlation with the dynamics of the measured fluxes. This study demonstrates that physiological remote sensing indices are required for monitoring gross primary production when standard vegetation indices associated with structure are insensitive to the seasonal dynamics of the vegetation.

## Acknowledgments

The authors gratefully acknowledge the financial support from the Spanish Ministry of Science and Education (MEC) for projects AGL2009-13105, CONSOLIDER RIDECO (CSD2006-67) and from the Regional Government of Andalusia for project P08-AGR-04202. A. Morales held a postgraduate fellowship granted by *Fundación Caja Madrid*. I. Calatrava, R. del Río, and J. L. Vazquez provided technical assistance with the eddy covariance measurements. D. Notario, A. Vera, A. Hornero, and R. Romero are also acknowledged for their technical support during the field and airborne campaigns.

## References

- Asrar, G., Fuchs, M., Kanemasu, E. T., & Hatfield, J. L. (1984). Estimating absorbed photosynthetic radiation and leaf area index from spectral reflectance in wheat. *Agronomy Journal*, 76, 300–306.
- Baldocchi, D. D. (2003). Assessing the eddy covariance technique for evaluating carbon dioxide exchange rates of ecosystems: past, present and future. *Global Change Biology*, 9, 479–492.
- Baret, F., & Guyot, G. (1991). Potentials and limits of vegetation indices for LAI and APAR assessment. *Remote Sensing of Environment*, 35, 161–173.
- Bélisle, C. J. P. (1992). Convergence theorems for a class of simulated annealing algorithms on  $R^d$ . *Journal of Applied Probability*, 29(4), 885–895.
- Berni, J. A. J., Zarco-Tejada, P. J., Suárez, L., & Fereres, E. (2009). Thermal and narrow-band multispectral remote sensing for vegetation monitoring from an unmanned aerial vehicle. *IEEE Transactions on Geoscience and Remote Sensing*, 47(3), 722–738.
- Bolker, B. M., & R Development Core Team (2012). *bbmle: Tools for general maximum likelihood estimation*. <http://cran.r-project.org/web/packages/bbmle/>
- Broge, N. H., & Leblanc, E. (2000). Comparing prediction power and stability of broad-band and hyperspectral vegetation indices for estimation of green leaf area index and canopy chlorophyll density. *Remote Sensing of Environment*, 76, 156–172.
- Damm, A., Elbers, J., Erler, E., Gioli, B., Hamdi, K., Hutjes, R., et al. (2010). Remote sensing of sun induced fluorescence to improve modeling of diurnal courses of gross primary production (GPP). *Global Change Biology*, 16, 171–186.
- Damm, A., Erler, A., Hillen, W., Meroni, M., Schaepman, M. E., Verhoef, W., et al. (2011). Modeling the impact of spectral sensor configurations on the FLD retrieval accuracy of sun-induced chlorophyll fluorescence. *Remote Sensing of Environment*, 115, 1882–1892.
- Dobrowski, S. Z., Pusknik, J. C., Zarco-Tejada, P. J., & Ustin, S. L. (2005). Simple reflectance indices track heat and water stress induced changes in steady state chlorophyll fluorescence. *Remote Sensing of Environment*, 97(3), 403–414.

- European Space Agency (2008). *ESA SP-1313/4 candidate earth explorer core missions – Reports for assessment: FLEX-Fluorescence EXplorer*. Noordwijk, The Netherlands: ESA Communication Production Office (available on line at [http://esamultimedia.esa.int/docs/SP1313-4\\_FLEX.pdf](http://esamultimedia.esa.int/docs/SP1313-4_FLEX.pdf))
- Flexas, J., Briantais, J. M., Cerovic, Z., Medrano, H., & Moya, I. (2000). Steady-state and maximum chlorophyll fluorescence responses to water stress in grapevine leaves: A new remote sensing system. *Remote Sensing of Environment*, 73, 282–297.
- Flexas, J., Escalona, J. M., Evain, S., Gulias, J., Moya, I., Osmond, C. B., et al. (2002). Steady-state chlorophyll fluorescence ( $F_s$ ) measurements as a tool to follow variations of net  $\text{CO}_2$  assimilation and stomatal conductance during water-stress in C-3 plants. *Physiologia Plantarum*, 114(2), 231–240.
- Foken, T., Gockede, M., Mauder, M., Lahr, L., Amiro, B., & Munger, W. (2004). Post-field data quality control. In X. Lee, W. Massman, & B. Law (Eds.), *Handbook of micrometeorology. Atmospheric and oceanographic sciences library*. (pp. 181–208). Netherlands: Springer.
- Frankenberg, C., Fisher, J. B., Worden, J., Badgley, G., Saatchi, S. S., Lee, J. E., et al. (2011). New global observations of the terrestrial carbon cycle from GOSAT: Patterns of plant fluorescence with gross primary productivity. *Geophysical Research Letters*, 38, L17706. <http://dx.doi.org/10.1029/2011GL048738>.
- Fuchs, M. (1990). Infrared measurement of canopy temperature and detection of plant water stress. *Theoretical and Applied Climatology*, 42(4), 253–261.
- Fung, Y., Tucker, C. J., & Prentice, K. C. (1987). Application of advanced very high resolution radiometer vegetation index to study atmosphere–biosphere exchange of  $\text{CO}_2$ . *Journal of Geophysical Research*, 92, 2999–3015.
- Gamon, J. A., Peñuelas, J., & Field, C. B. (1992). A narrow-wave band spectral index that tracks diurnal changes in photosynthetic efficiency. *Remote Sensing of Environment*, 41, 35–44.
- Gardner, B. R., Blad, B. L., & Watts, D. G. (1981). Plant and air temperatures in differentially-irrigated corn. *Agricultural Meteorology*, 25(C), 207–217.
- Gockede, M., Foken, T., Aubinet, M., Aurela, M., Banza, J., Bernhofe, C., et al. (2008). Quality control of CarboEurope flux data – Part 1: Coupling footprint analyses with flux data quality assessment to evaluate sites in forest ecosystems. *Biogeosciences*, 5(2), 433–450.
- Gómez, J. A., Zarco-Tejada, P. J., García-Morillo, J., Gama, J., & Soriano, M. A. (2011). Determining biophysical parameters on olive trees using CASI airborne and QuickBird satellite imagery. *Agronomy Journal*, 103(3), 644–654.
- González-Dugo, V., Zarco-Tejada, P. J., Berni, J. A., Suárez, L., Goldammer, D., & Fereres, E. (2012). Almond tree canopy temperature reveals intra-crown variability that is water stress-dependent. *Agricultural and Forest Meteorology*, 154–155, 156–165.
- Goward, S. N., & Huemmrich, K. F. (1992). Vegetation canopy PAR absorptance and the normalized difference vegetation index: An assessment using the SAIL model. *Remote Sensing of Environment*, 39, 119–140.
- Guanter, L., Alonso, L., Gomez-Chova, L., Meroni, M., Preusker, R., & Fischer, J. (2010). Developments for vegetation fluorescence retrieval from spaceborne high resolution spectrometry in the  $\text{O}_2\text{-A}$  and  $\text{O}_2\text{-B}$  absorption bands. *Journal of Geophysical Research-Atmospheres*, 115.
- Guanter, L., Frankenberg, C., Dudhia, A., Lewis, P. E., Gomez-Dans, J., Kuze, A., et al. (2012). Retrieval and global assessment of terrestrial chlorophyll fluorescence from GOSAT space measurements. *Remote Sensing of Environment*, 121, 236–251.
- Haboudane, D., Miller, J. R., Pattey, E., Zarco-Tejada, P. J., & Strachan, I. (2004). Hyperspectral vegetation indices and novel algorithms for predicting green LAI of crop canopies: Modeling and validation in the context of precision agriculture. *Remote Sensing of Environment*, 90(3), 337–352.
- Haboudane, D., Miller, J. R., Tremblay, N., Zarco-Tejada, P. J., & Dextraze, L. (2002). Integrated narrow-band vegetation indices for prediction of crop chlorophyll content for application to precision agriculture. *Remote Sensing of Environment*, 84, 416–426.
- Hernández-Clemente, R., Navarro-Cerrillo, R., Suárez, L., Morales, F., & Zarco-Tejada, P. J. (2011). Assessing structural effects on PRI for stress detection in conifer forests. *Remote Sensing of Environment*, 115(9), 2360–2375.
- Huete, A., Didan, K., Miura, T., Rodriguez, E. P., Gao, X., & Ferreira, L. G. (2002). Overview of the radiometric and biophysical performance of the MODIS vegetation indices. *Remote Sensing of Environment*, 83, 195–213.
- Huete, A. R., Didan, K., Shimabukuro, Y. E., Ratana, P., Saleska, S. R., Hutrya, L. R., et al. (2006). Amazon rainforests green-up with sunlight in dry season. *Geophysical Research Letters*, 33, L06405. <http://dx.doi.org/10.1029/2005GL025583>.
- Jiang, Z., Huete, A. R., Didan, K., & Miura, T. (2008). Development of a two-band enhanced vegetation index without a blue band. *Remote Sensing of Environment*, 112(10), 3833–3845.
- Joiner, J., Yoshida, Y., Vasilkov, A. P., Yoshida, Y., Corp, L. A., & Middleton, E. M. (2011). First observations of global and seasonal terrestrial chlorophyll fluorescence from space. *Biogeosciences*, 8(3), 637–651.
- Justice, C. O., Townshend, J. R. G., Holben, B. N., & Tucker, C. J. (1985). Analysis of the phenology of global vegetation using meteorological satellite data. *International Journal of Remote Sensing*, 6, 1271–1318.
- Kormann, R., & Meixner, F. X. (2001). An analytical footprint model for non-neutral stratification. *Boundary-Layer Meteorology*, 99(2), 207–224.
- Krause, G. H., & Weis, E. (1984). Chlorophyll fluorescence as a tool in plant physiology. II. Interpretation of fluorescence signals. *Photosynthesis Research*, 5, 139–157.
- Kuze, A., Suto, H., Nakajima, M., & Hamazaki, T. (2009). Thermal and near infrared sensor for carbon observation Fourier-transform spectrometer on the greenhouse gases observing satellite for greenhouse gases monitoring. *Applied Optics*, 48, 6716–6733.
- Leinonen, I., & Jones, H. G. (2004). Combining thermal and visible imagery for estimating canopy temperature and identifying plant stress. *Journal of Experimental Botany*, 55(401), 1423–1431.
- Lichtenthaler, H. K., & Rinderle, U. (1988). The role of chlorophyll fluorescence in the detection of stress conditions in plants. *CRC Critical Reviews in Analytical Chemistry*, 19(Suppl. 1), 529–585.
- Malenovsky, Z., Mishra, K. B., Zemek, F., Rascher, U., & Nebal, L. (2009). Scientific and technical challenges in remote sensing of plant canopy reflectance and fluorescence. *Journal of Experimental Botany*, 60, 2987–3000.
- Mauder, M., & Foken, T. (2011). *Eddy-Covariance Software Package TK3*. University of Bayreuth ([http://www.bayceer.uni-bayreuth.de/mm/de/software/software/software\\_dl.php](http://www.bayceer.uni-bayreuth.de/mm/de/software/software/software_dl.php))
- Meroni, M., Busetto, L., Colombo, R., Guanter, L., Moreno, J., & Verhoef, W. (2010). Performance of spectral fitting methods for vegetation fluorescence quantification. *Remote Sensing of Environment*, 114, 363–374.
- Meroni, M., Picchi, V., Rossini, M., Cogliati, S., Panigada, C., Nali, C., et al. (2008). Leaf level early assessment of ozone injuries by passive fluorescence and PRI. *International Journal of Remote Sensing*, 29(17), 5409–5422.
- Meroni, M., Rossini, M., Guanter, L., Alonso, L., Rascher, U., & Colombo, R. (2009). Remote sensing of solar-induced chlorophyll fluorescence: Review of methods and applications. *Remote Sensing of Environment*, 113, 2037–2051.
- Meroni, M., Rossini, M., Picchi, V., Panigada, C., Cogliati, S., Nali, C., et al. (2008). Assessing steady-state fluorescence and PRI from hyperspectral proximal sensing as early indicators of plant stress: The case of ozone exposure. *Sensors*, 8, 1740–1754.
- Moller, M., Alchanatis, V., Cohen, Y., Meron, M., Tsipris, J., Naor, A., et al. (2007). Use of thermal and visible imagery for estimating crop water status of irrigated grapevine. *Journal of Experimental Botany*, 58(4), 827–838.
- Moya, I., Camenen, L., Evain, S., Goulas, Y., Cerovic, Z. G., & Latouche, G. (2004). A new instrument for passive remote sensing 1. Measurements of sunlight-induced chlorophyll fluorescence. *Remote Sensing of Environment*, 91, 186–197.
- Muraoka, H., & Koizumi, H. (2005). Photosynthetic and structural characteristics of canopy and shrub trees in a cool-temperate deciduous broadleaved forest: implication to the ecosystem carbon gain. *Agricultural and Forest Meteorology*, 134, 39–59.
- Nagai, S., Saigusa, N., Muraoka, H., & Nishida Nasahara, K. (2010). What makes the satellite-based EVI–GPP relationship unclear in a deciduous broad-leaved forest? *Ecological Research*, 25, 359–365.
- Papageorgiou, G. (1975). Chlorophyll fluorescence: An intrinsic probe of photosynthesis. In Govindjee (Ed.), *Bioenergetics of photosynthesis* (pp. 319–371). New York: Academic Press.
- Peguero-Pina, J. J., Morales, F., Flexas, J., Gil-Pelegrín, E., & Moya, I. (2008). Photochemistry, remotely sensed physiological reflectance index and de-epoxidation state of the xanthophyll cycle in *Quercus coccifera* under intense drought. *Oecologia*, 156(1), 1–11.
- Pérez-Priego, O., Zarco-Tejada, P. J., Sepulcre-Cantó, G., Miller, J. R., & Fereres, E. (2005). Detection of water stress in orchard trees with a high-resolution spectrometer through chlorophyll fluorescence in-filling of the  $\text{O}_2\text{-A}$  band. *IEEE Transactions on Geoscience and Remote Sensing*, 43, 2860–2869.
- Plascyk, J. A., & Gabriel, F. C. (1975). The fraunhofer line discriminator MKII – An airborne instrument for precise and standardized ecological luminescence measurement. *IEEE Transactions on Instrumentation and Measurement*, IM-24, 306–313.
- Porcar-Castell, A. (2011). A high-resolution portrait of the annual dynamics of photochemical and non photochemical quenching in needles of *Pinus sylvestris*. *Physiologia Plantarum*, 143(2), 139–153.
- Press, W. H., Teukolsky, S. A., Vetterling, W. T., & Flannery, B. P. (2007). *Numerical recipes: The art of scientific computing*. Cambridge University Press.
- Prince, S. D. (1991). A model of regional primary production for use with coarse resolution satellite data. *International Journal of Remote Sensing*, 12(6), 1313–1330.
- Rascher, U., Agati, G., Alonso, L., Cecchi, G., Champagne, S., Colombo, R., et al. (2009). CELES2: The remote sensing component to quantify photosynthetic efficiency from the leaf to the region by measuring sun-induced fluorescence in the oxygen absorption bands. *Biogeosciences Discussions*, 6(7), 2217–2266.
- Richardson, A. D., Mahecha, M. D., Falge, E., Kattge, J., Moffat, A. M., Papale, D., et al. (2008). Statistical properties of random  $\text{CO}_2$  flux measurement uncertainty inferred from model residuals. *Agricultural and Forest Meteorology*, 148(1), 38–50.
- Rougean, J. L., & Breon, F. M. (1995). Estimating PAR absorbed by vegetation from bidirectional reflectance measurements. *Remote Sensing of Environment*, 51, 375–384.
- Rouse, J. W., Haas, R. H., Schell, J. A., Deering, D. W., & Harlan, J. C. (1974). Monitoring the vernal advancements and retrogradation of natural vegetation. In MD, & U.G. (Eds.), *Nasa/Gscf Final Report* (pp. 371).
- Running, S. W., Baldocchi, D. D., Turner, D. P., Gower, S. T., Bakwin, P. S., & Hibbard, K. A. (1999). A global terrestrial monitoring network integrating tower fluxes, flask sampling, ecosystem modeling and EOS satellite data. *Remote Sensing of Environment*, 70(1), 108–127.
- Running, S. W., & Nemani, R. R. (1988). Relating seasonal patterns of the AVHRR vegetation index to simulated photosynthesis and transpiration of forest in different climates. *Remote Sensing of Environment*, 24, 347–367.
- Running, S. W., Nemani, R. R., Peterson, D. L., Band, L. E., Potts, D. F., Pierce, L. L., et al. (1989). Mapping regional forest evapotranspiration and photosynthesis by coupling satellite data with ecosystem simulation. *Ecology*, 70, 1090–1101.
- Sellers, P. J. (1985). Canopy reflectance, photosynthesis and transpiration. *International Journal of Remote Sensing*, 6, 1335–1372.
- Sims, D. A., Rahman, A. F., Cordova, V. D., El-Masri, B. Z., Baldocchi, D. D., Bolstad, P. V., et al. (2008). A new model of gross primary productivity for North American ecosystems based solely on the enhanced vegetation index and land surface temperature from MODIS. *Remote Sensing of Environment*, 112, 1633–1646.
- Soukupová, J., Cséfalvay, L., Urban, O., Kosvancová, M., Marek, M., Rascher, U., et al. (2008). Annual variation of the steady-state chlorophyll fluorescence emission of evergreen plants in temperate zone. *Functional Plant Biology*, 35, 63–76.
- Suárez, L., Zarco-Tejada, P. J., Berni, J. A. J., González-Dugo, V., & Fereres, E. (2009). Modelling PRI for water stress detection using radiative transfer models. *Remote Sensing of Environment*, 113, 730–744.

- Suárez, L., Zarco-Tejada, P. J., González-Dugo, V., Berni, J. A. J., Sagardoy, R., Morales, F., et al. (2010). Detecting water stress effects on fruit quality in orchards with time-series PRI airborne imagery. *Remote Sensing of Environment*, 114, 286–298.
- Suárez, L., Zarco-Tejada, P. J., Sepulcre-Cantó, G., Pérez-Priego, O., Miller, J. R., Jiménez-Muñoz, J. C., et al. (2008). Assessing canopy PRI for water stress detection with diurnal airborne imagery. *Remote Sensing of Environment*, 112, 560–575.
- Testi, L., Orgaz, F., & Villalobos, F. J. (2006). Variations in bulk canopy conductance of an irrigated olive (*Olea europaea* L.) orchard. *Environmental and Experimental Botany*, 55(1–2), 15–28.
- Thenot, F., Méthy, M., & Winkel, T. (2002). The photochemical reflectance index (PRI) as a water-stress index. *International Journal of Remote Sensing*, 23(23), 5135–5139.
- Tucker, C. J., & Sellers, P. J. (1986). Satellite remote sensing of primary productivity. *International Journal of Remote Sensing*, 7, 1395–1416.
- Vogelmann, J. E., Rock, B. N., & Moss, D. M. (1993). Red edge spectral measurements from sugar maple leaves. *International Journal of Remote Sensing*, 14, 1563–1575.
- Zarco-Tejada, P. J., Berjón, A., López-Lozano, R., Miller, J. R., Marin, P., Cachorro, V., et al. (2005). Assessing vineyard condition with hyperspectral indices: Leaf and canopy reflectance simulation in a row-structured discontinuous canopy. *Remote Sensing of Environment*, 99, 271–287.
- Zarco-Tejada, P. J., Berni, J. A. J., Suárez, L., Sepulcre-Cantó, G., Morales, F., & Miller, J. R. (2009). Imaging chlorophyll fluorescence from an airborne narrow-band multispectral camera for vegetation stress detection. *Remote Sensing of Environment*, 113, 1262–1275.
- Zarco-Tejada, P. J., Catalina, A., González, M. R., & Martín, P. (submitted for publication). Relationships between net photosynthesis and steady-state chlorophyll fluorescence retrieved from airborne hyperspectral imagery. *Remote Sensing of Environment*.
- Zarco-Tejada, P. J., González Dugo, V., & Berni, J. A. J. (2012). Fluorescence, temperature and narrowband indices acquired from a UAV platform for water stress detection using a micro-hyperspectral imager and a thermal camera. *Remote Sensing of Environment*, 117, 322–337.
- Zarco-Tejada, P. J., Miller, J. R., Mohammed, G. H., Noland, T. L., & Sampson, P. H. (2001). Scaling-up and model inversion methods with narrow-band optical indices for chlorophyll content estimation in closed forest canopies with hyperspectral data. *IEEE Transactions on Geoscience and Remote Sensing*, 39(7), 1491–1507.
- Zarco-Tejada, P. J., Miller, J. R., Morales, A., Berjón, A., & Agüera, J. (2004). Hyperspectral indices and model simulation for chlorophyll estimation in open-canopy tree crops. *Remote Sensing of Environment*, 90(4), 463–476.
- Zarco-Tejada, P. J., Pushnik, J., Dobrowski, S., & Ustin, S. L. (2003). Steady-state chlorophyll a fluorescence detection from canopy derivative reflectance and double-peak red-edge effects. *Remote Sensing of Environment*, 84(2), 283–294.
- Zarco-Tejada, P. J., Suárez, L., & González-Dugo, V. (submitted for publication). Spatial resolution effects on chlorophyll fluorescence retrievals in a heterogeneous canopy using hyperspectral imagery and radiative transfer simulation. *Geoscience and Remote Sensing Letters*.